Annals of Nuclear Medicine Vol. 14, No. 4, 279–284, 2000

Fundamental study of hot spot detectability in 3-dimensional positron emission tomography

Hong ZHANG,* Tomio INOUE,* Saleh ALYAFEI,* Mei TIAN,** Noboru ORIUCHI,* Akihiro ICHIKAWA,* Kunio MATSUBARA* and Keigo ENDO*

*Department of Diagnostic Radiology and Nuclear Medicine, Gunma University School of Medicine, Gunma, Japan
**Department of Nuclear Medicine, First Hospital of Shanxi Medical University, Shanxi, People's Republic of China

The purpose of this study was to investigate the detectability of small hot lesions with the 3-dimensional transmission/emission (3D T/E) acquisition mode in FDG-PET scan. The correlation of target detectability, target size, target to non-target uptake ratio (T/N ratio) and standardized uptake value (SUV) were studied. Small hot lesions ranged from 4.4 mm to 36.9 mm in diameter were located in cylindrical phantom. The images of phantoms with a T/N ratio of 2.0, 4.0, 6.0, 8.0, 9.6, 13.2, 17.5, 23.8 and 30.3 were obtained with 2-dimensional transmission/emission (2D T/E) scan and 3D T/E scans. Targets in diameter more than 10.6 mm in diameter with an actual T/N ratio ranged from 6.0 to 30.3 could be identified on the images obtained with all the 2D T/E and 3D T/E acquisition modes. The detectability efficiency of small hot target in 2D T/E and 3D T/E scans was as same (77.8%). The T/N ratio of targets from 2D T/E images was 30% to 48.4% different to that from 3D T/E image, and the SUV of the target from the 2D T/E images was almost the same as that from 3D T/E images. This study revealed that 3D T/E scanning had similar hot spot detectability to 2D T/E scanning; 3D T/E and 2D T/E scanning had the same faculty for semi-quantitative analysis using SUV. These findings may be helpful for the diagnosis and understanding of 3D T/E FDG-PET in hot lesion detection.

Key words: 2-dimensional and 3-dimensional PET; T/N ratio; SUV; hot spot detectability

INTRODUCTION

PET STUDIES with 2-(fluorine-18)fluoro-2-deoxy-D-glucose (FDG) is one of the several metabolic imaging procedures being used to detect various diseases.[1] Recently, FDG-PET studies have been proven to be of significant clinical feasibility in oncology, since the malignant potential of a lesion can be defined by the degree of ^{18}F-FDG accumulation within the lesion.[2,3]

In detecting hot spot lesions in nuclear oncology, a high target to non-target (T/N) ratio of a tumor-seeking agent implies the aggressiveness or the high malignancy of the lesion,[4] and a decrease in the T/N ratio indicates a good response to treatment.[5] Also the standardized uptake value (SUV) has been widely used as a useful objective index for differentiating malignant lesions from benign lesions[6] and monitoring the effects of therapy on a malignant lesion.[7] In most FDG-PET studies, ability of PET to detect tumors was assessed by using 2-dimensional (2D) data acquisitions and human subjects. The advent of 3-dimensional (3D) data acquisition hardware and reconstruction software has significantly increased the detection sensitivity of PET scan compared with the conventional 2D systems. Although clinical 3D mode FDG-PET demonstrated feasibility in detecting tumors,[8,9] the limitations of 3D FDG-PET have not been fully explored: for example, what is the minimum size and T/N ratio of a tumor detectable with FDG-PET? How effective is 3D FDG-PET in detecting small lesions compared with 2D? How quantifiable is 3D FDG-PET in detecting small tumors compared with 2D? There is little literature on whether and how the lesion volume affects the T/N ratio and SUV; and the influence of the partial

Received February 7, 2000, revision accepted June 1, 2000.
For reprint contact: Hong Zhang, Ph.D., Department of Diagnostic Radiology and Nuclear Medicine, Gunma University School of Medicine, Showa-machi 3–39–22, Maebashi 371–8511, JAPAN.
E-mail: zhang@med.gunma-u.ac.jp

volume effect is not fully discussed in the quantification of tumor uptake by the 3D imaging techniques, especially in detecting tumors with FDG-PET. The aim of this study was to evaluate detectability in the 3D T/E acquisition mode of an FDG-PET study in detecting small hot lesions with special reference to lesion size, T/N uptake ratio and SUV by using a SET-2400W PET scanner.

MATERIALS AND METHODS

Performance of Shimadzu SET-2400W

The SET 2400W (Shimadzu, Kyoto, Japan) is a newly designed whole-body PET scanner with a large axial field of view (20 cm). The scanner consists of four rings of 112 BGO detector units (22.8 mm in-plane × 50 mm axial × 30 mm depth). Each detector unit has a 6 (in-plane) × 8 (axial) matrix of BGO crystals coupled to two dual photomultiplier tubes (Hamamatsu R1548). Crystal size is 3.8 mm (in-plane), 6.25 mm (axial) and 30 mm (depth). These are arranged in 32 rings with 672 crystals each, giving 63 two-dimensional image planes. The axial FOV is 20 cm. The ring diameter is 850 mm and the patient port diameter is 590 mm. Signals from the photomultiplier tubes are processed to the position of the crystal in which the gamma photon hits it by using a coincidence time window of 15 ns. Position non-linearity and energy non-uniformity of the detector unit are corrected in real time. In the 2D mode, axial coincidence path acceptance can be controlled from 1 to 8 to optimize sensitivity and axial resolution. The system has content septa 1 mm thick and 55 mm long for the 2D mode. The septa can be automatically retracted for the 3D mode. 63 sinograms are stored in a large scale acquisition memory (1 GB) in the 2D mode. In the 3D mode, all possible coincidence pairs of 1,024 sinograms are stored in the same memory. A dead time correction and physical decay correction of radioisotope can be performed in real time in the memory.[10,11] A ^{68}Ge-^{68}Ga external rod source with 185 MBq can be orbited in a 640 mm radius to measure blank scan and transmission scan data. The major aspects of the system construction and performance are listed in Tables 1[12] and 2.[13]

With the developments of imaging technology, the scans in 2D and 3D modes have been available in SET 2400W, mainly in 2D (Transmission + Emission) and 3D (Transmission + Emission) modes.

Phantom studies

All the measurements were performed on a hot spot phantom: a 20 cm diameter and 18.5 cm high cylinder containing six smaller columns 4.4, 6.3, 10.6, 16.3, 22.6 and 36.9 mm in diameter, as it is more representative of the imaging quality associated with clinical scanning and easier to investigate the influence of lesion size, T/N ratio and lesion location on the detectability of PET. The phantom was placed on the bed and centered within the field of view. By using a phantom containing six columns filled with a solution of ^{18}F-FDG, nine times separate acquisitions were performed with the concentration adjusted to provide lesion to background concentration ratios of 2.0 : 1, 4.0 : 1, 6.0 : 1, 8.0 : 1, 9.6 : 1, 13.2 : 1, 17.5 : 1, 23.8 : 1 and 30.3 : 1, to simulate varying clinical situations for detecting hot lesions in both of 2D and 3D modes with SET-2400 PET. Since the experiments were assumed to be in clinical conditions, the concentration of the background in phantom was calculated and set at 3.7 kBq/m*l* (ID/g), as in the case of a typical clinical admin-

Table 1 System major parameters of SET-2400W

Block detector design	6 (in-plane) × 8 (axial)
Number of rings	32 rings
Number of slices	63 slices
Number of detector blocks	448
Crystal size (mm^3)	3.8 × 6.25 × 30
Number of crystals	21,504
Image plane spacing (mm)	3,125
Detector ring diameter (mm)	850
Patient aperture (mm)	595
Field of view (mm)	
Axial	200
Transverse	590
For whole body scan	1,750

Table 2 Performance data in 2D and 3D mode

	2D		3D	
Spatial resolution (FWHM: mm)	4.4 (r = 0 cm) 5.9 (r = 20 cm)		4.7 (r = 0 cm) 7.6 (r = 20 cm)	
Total sensitivity (kcps/kBq/m*l*)	7.98		48.95	
Average scatter fraction (%)	13.1		30.1	
NECR	73	28.3	86.1	5.8
kcps kBq/m*l*				

NERC: Noise-equivalent count rate

Table 3 Results of detectability of small hot lesion on phantom's reconstructed PET images in 2D T/E and 3D T/E mode

T/N ratio	Target size (Diameter: mm)											
	4.4		6.3		10.6		16.3		22.5		36.9	
	a	b	a	b	a	b	a	b	a	b	a	b
2.0	−	−	−	−	−	−	±	−	+	+	+	+
4.0	−	−	−	−	+	±	+	+	+	+	+	+
6.0	−	−	−	−	+	+	+	+	+	+	+	+
8.0	−	−	±	±	+	+	+	+	+	+	+	+
9.6	−	−	+	+	+	+	+	+	+	+	+	+
13.2	±	+	+	+	+	+	+	+	+	+	+	+
17.5	+	+	+	+	+	+	+	+	+	+	+	+
23.8	+	+	+	+	+	+	+	+	+	+	+	+
30.3	+	+	+	+	+	+	+	+	+	+	+	+

+: Hot lesion is identified; −: not identified; ±: uncertain
a: 2D T/E mode; b: 3D T/E mode

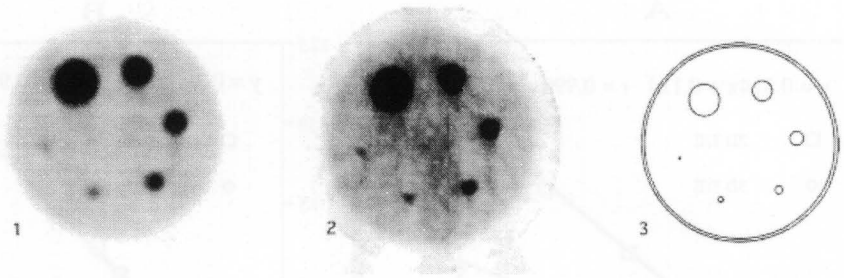

Fig. 1 Images of the hot spot phantom in 2D T/E (1) and 3D T/E (2) scanning with an actual T/N ratio of 30.3. The line drawing of (3) indicates the relative size and position of columns containing FDG solution.

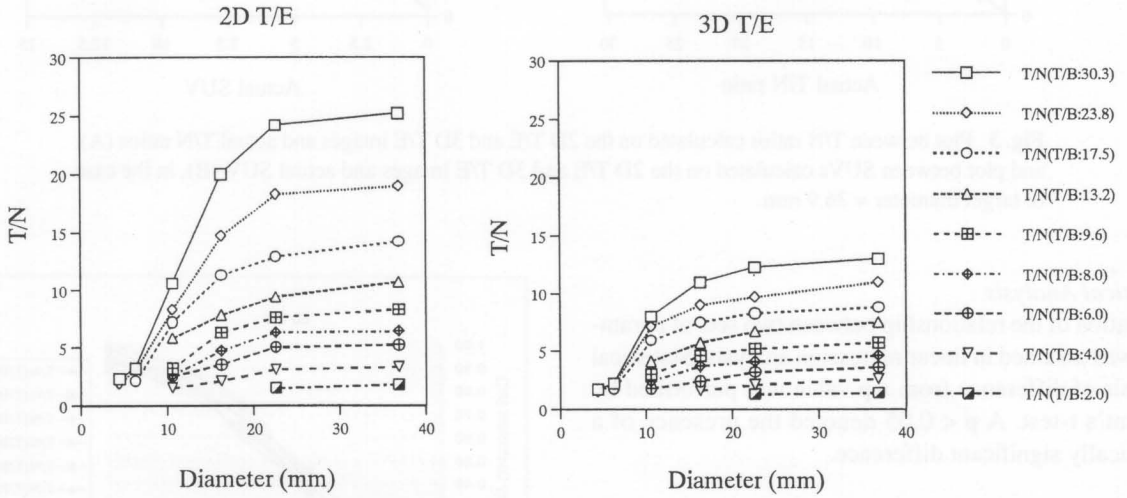

Fig. 2 Correlations between target size and T/N ratio of target in 2D T/E and 3D T/E images.

istration of 185 MBq FDG administrated to a person with a normal weight of 60 kg, and the gravity of the tumor and background muscle was assumed as 1 g/m*l*.[14]

To conduct the measured attenuation correction for the 2D T/E and 3D T/E, 2D transmission scans with an external ^{68}Ge-^{68}Ga rod source were performed for 10 min before FDG administration. After administration of FDG, emission data were acquired in the 2D and 3D modes for 6 and 2 min, respectively. So the transmission scan of all the 2D T/E and 3D T/E scans in this paper means 2D transmission scan.

Quantitative analysis

The ordered subsets expectation maximization (OS-EM) algorithm was used to reconstruct the attenuation-corrected 2D and 3D emission data. The conventional EM algorithm (a special case of OS-EM with the number of subsets equal to 1) was used for 2D imaging and the OS-EM algorithm with a subsets equal to 32, iterations equal to 1 was used for 3D imaging. The images were reconstructed in a 128 × 128 matrix. The reconstructed images used in this study were all corrected with attenuation images. The functional images of SUV was also produced. In this study, T/N ratio, SUV and recovery coefficient (RC) were defined as:

$$\text{T/N ratio} = \frac{\text{mean pixel counts in target}}{\text{mean pixel counts in background}}$$

$$\text{SUV} = \frac{\text{radioactive concentration in target (MBq/m}l\text{)}}{\text{injected dose (MBq)/water weight in phantom (m}l\text{)}}$$

$$\text{RC} = \frac{\text{apparent radioactive concentration in target (MBq/m}l\text{)}}{\text{true radioactive concentration in target (MBq/m}l\text{)}}$$

Region of interest (ROI) analysis was employed to examine the quantitative bias in 2D T/E and 3D T/E reconstructed images. A sequences of transverse images were viewed by two nuclear physicians. A target was defined as a focus of increased FDG uptake above the intensity of the surrounding activity. ROIs were drawn on areas corresponding to the targets. The highest point of radioactivity was included in these ROIs. Also a 30 mm diameter ROI was marked on the center of the phantom for background counts. The visual evaluations of the detectability of targets in the phantom were identified (+), not identified (−) and uncertain (±).

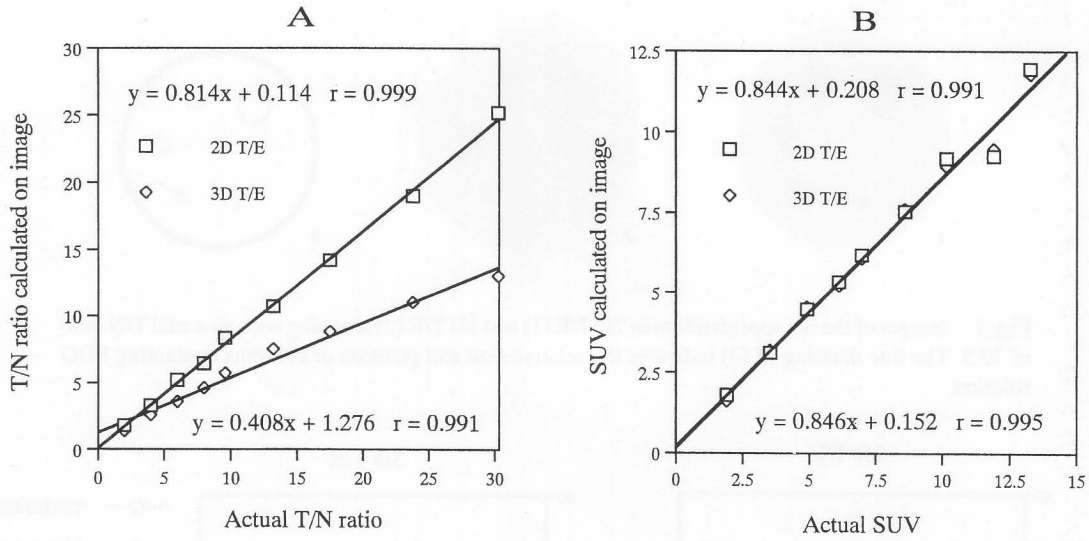

Fig. 3 Plot between T/N ratios calculated on the 2D T/E and 3D T/E images and actual T/N ratios (A), and plot between SUVs calculated on the 2D T/E and 3D T/E images and actual SUV (B), in the case of target diameter = 36.9 mm.

Statistical Analysis

Evaluation of the relationship between two sets of parameters was assumed in linear regression analysis. Statistical analysis of difference from a p value was performed by Student's t-test. A $p < 0.05$ denoted the presence of a statistically significant difference.

RESULTS

The images of the phantom acquired in the 2D T/E and 3D T/E modes are shown in Figure 1. The image quality obatined in 2D T/E mode was apparently better than that in the 3D T/E mode, but the 3D image revealed the small hot lesion well even if the image contrast was not very good (Fig. 1). The T/N ratio in the 2D T/E image was 30% to 48.4% higher than that in the 3D T/E image with the same actual T/N (Fig. 2). The relationships among the T/N ratio and SUV calculated on the 2D T/E and 3D T/E PET images were examined. The data for a target 36.9 mm in diameter are shown (Fig. 3). There were strong positive correlations between the T/N ratio calculated on the image and the actual T/N ratio in the 2D T/E and 3D T/E modes ($r = 0.999$, 0.991, $p < 0.001$). There were also strong positive correlations between the SUV calculated on the image and the actual SUV in the 2D T/E and 3D T/E modes ($r = 0.991$, 0.995, $p < 0.001$), but the T/N ratios derived from the 3D T/E image were significantly lower than those derived from the 2D T/E image (Fig. 3).

The RCs of the targets in the reconstructed images with actual T/N ratios from 2.0 to 30.3 were calculated versus the target size as shown in Figure 4. There were no significant differences in RC within actual T/N ratios ranging from 2.0 to 30.3 in any of the visible targets on the 2D T/E and 3D T/E images. Therefore, one normalized

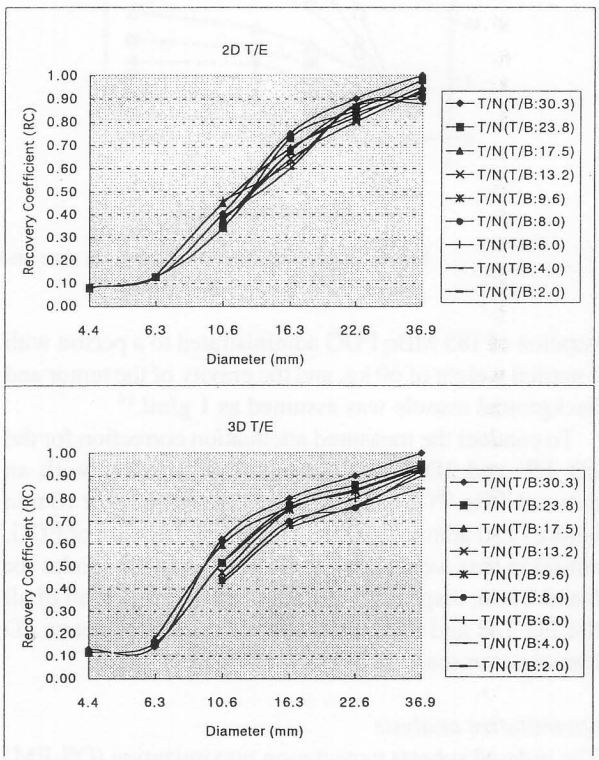

Fig. 4 RCs as a function of target diameter with actual T/N ratio ranged from 2.0 to 30.3 on the 2D T/E and 3D T/E images.

RC line independent of the actual T/N ratio for any target size could result in both 2D T/E, and 3D T/E modes.

The relationships among the SUV of targets calculated on the 2D T/E and 3D T/E images were also examined (Fig. 5). There was good agreement for any size target with actual SUVs ranging from 1.92 to 13.28 in 2D T/E

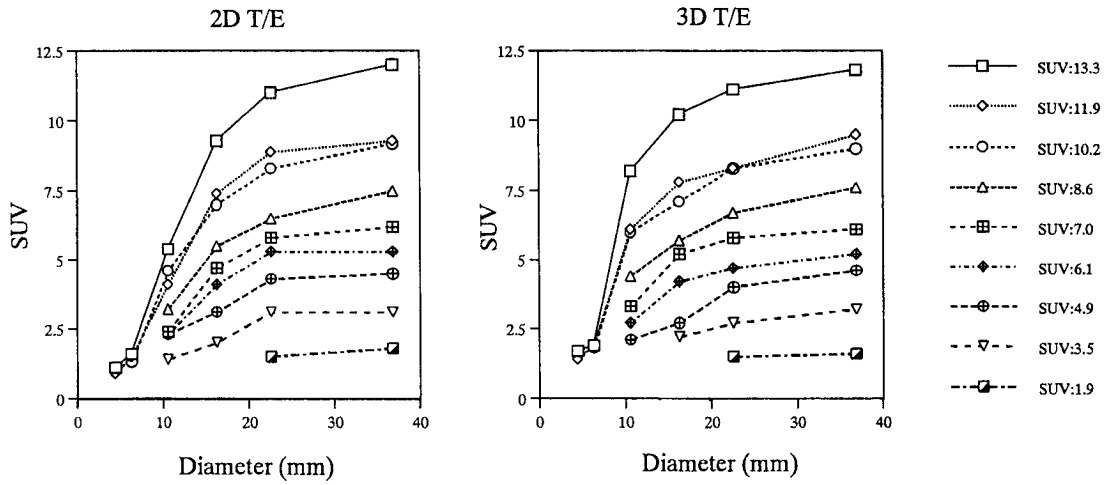

Fig. 5 Correlations between target size and SUV of target ranged from 1.9 to 13.3 in 2D T/E and 3D T/E images.

and 3D T/E images.

The visual interpretation of targets with T/N ratios ranging from 2.0 to 30.3 in 2D T/E and 3D T/E images are summarized in Table 3. Targets (Diameter ≥ 10.6 mm) with an actual T/N ratio ranging from 6.0 to 30.3 could be identified in both the 2D T/E and 3D T/E images. All the targets with an actual T/N ratio of more than 17.5 could be identified on 2D T/E and 3D T/E images. The detectability of small hot targets in 2D T/E and 3D T/E images was the same: 77.8%.

DISCUSSION

In this study we investigated the detectability of small hot targets and the correlation between the T/N ratio, SUV and target size in 2D T/E and 3D T/E images. The OS-EM method was used for image reconstruction, since the OS-EM method is effective for accelerating the reconstruction of iterative images given by the algorithm of EM methods, and it provides a good S/N image. We therefore used the OS-EM method for image reconstruction in 3D. And in order to compare the 3D image with the 2D image, which was reconstructed by OS-EM, the reconstruction algorithm used for 2D and 3D image reconstruction was thought to be preferable. Our results showed equal detectability of small hot targets in 2D T/E and 3D T/E images, and quantification of 2D T/E was almost the same as that of 3D T/E, except for quantification by means of T/N ratio analysis (Fig. 3).

In ROI analysis, mean counts per pixel were used for T/N calculation, since it was less sensitive to high-frequency noise and gave results superior to maximum pixel values.[15]

The results in Figure 2 show how the partial volume effect (PVE) occurred in the 2D T/E mode, which were lower than that in the 3D T/E mode with approximately a 50% decrease. This is consistent with the visual interpretation of the phantom images (Fig. 1). This was because of the approximately 2.3 times higher scatter fraction in the 3D mode than that in 2D mode (Table 2). Even so, the hot targets in the 3D T/E image could be clearly identified, since sensitivity in the 3D mode was 6.1 times higher than that in 2D mode. Strong correlations were noted between T/N ratios calculated on images and actual T/N ratios in the 2D T/E and 3D T/E images (Fig. 3). Also strong correlations were noted between SUVs calculated on images and actual SUVs in the 2D T/E and 3D T/E images (Fig. 3). These findings suggested that in quantitative analysis by T/N ratio, the 2D T/E was much more suitable than the 3D T/E image. Nevertheless, in the quantitative analysis by SUV, the findings in Figures 3 and 5 suggest that quantitative capability in the 2D T/E and 3D T/E images was almost the same, which may be due to the background activity which was not considered in the SUV calculations.

Investigation of RC summarized in Figure 4 showed a tendency for the RC values to be independent of the actual T/N ratio with a target size from 4.4 to 36.9 mm. This is also may be due to the fact that the background activity was not considered in the RC calculations. A normalized RC line independent of the actual T/N ratio for any target size could result in 2D T/E and 3D T/E images. The RC in the 3D T/E mode was slightly higher than that in the 2D T/E, because of the high sensitivity in the 3D mode. The resulting RC values provided most of the information necessary to correct for size effects in the quantitative analysis of PET images.

The data for phantom experiments presented here indicate that the T/N ratio from 3D T/E images was lower than that from 2D T/E, and SUV of the target derived from 3D T/E is the same as that derived from 2D T/E images, suggesting good quantitating ability of the 3D T/E scan in SUV analysis and clinical feasibility because of its shorter scanning time.

In fact the phantom used in this paper should have a larger diameter, but no larger phantom with hot spots inside it was available at our institute. As one another practicable evaluation method, we used the hot spot phantom in this experiment. On the other hand, recently some practical methods have been available for scatter correction in the PET of 3D mode.[16] In our paper the data on the phantom experiment were not obtained with scatter correction, and superior results might have been obtained if the scatter had been corrected.

CONCLUSION

We investigated the detectabilities of 2D T/E and 3D T/E scanning for small hot targets with the reference to target size, T/N ratios and SUV by using a SET-2400W PET scanner. We confirmed that 3D T/E scanning has the same detectability as 2D T/E scanning. 3D T/E scanning will not be suitable for T/N ratio analysis, compared to 2D T/E scanning, unless the scatter of 3D T/E scanning is properly corrected. 2D T/E and 3D T/E scanning are equally suitable for semi-quantitative analysis with SUV. These findings may be helpful for the diagnosis and understanding of 2D T/E and 3D T/E FDG-PET in hot lesion detection.

REFERENCES

1. Coleman RE. Revealing biochemistry in a single image. *J Nucl Med* 36 (9): 32N–33N, 1995.
2. Okada J, Yoshikawa K, Itami M, Imaseki K, Uno K, Itami J, et al. Positron emission tomography using fluorine18-fluorodeoxyglucose in malignant lymphoma: a comparison with proliferative activity. *J Nucl Med* 33: 325–329, 1992.
3. Strauss LG, Clorius JH, Schlag P, Lehner B, Kimmig B, Engenhart R, et al. Recurrence of colorectal tumors: PET evaluation. *Radiology* 170: 329–332, 1989.
4. Black KL, Hawkins RA, Kim KT, Becker DP, Lerner C, Marciano D. Use of thallium-201 SPECT to quantitate malignancy grade of gliomas. *J Neurosurg* 71: 342–346, 1989.
5. Lin J, Leung W, Stephen KWH, Kumta SM, Metreweli C, Johnson PJ. Quantitative evaluation of thallium-201 uptake in predicting chemotherapeutic response of osteosarcoma. *Eur J Nucl Med* 22: 553–555, 1995.
6. Patz EF Jr, Lowe VJ, Hoffman JM, Paine SS, Harris LK, Goodman PC. Persistent or recurrent brochogenic carcinoma: Detection with PET and 2-[F-18]-2-deoxy-D-glucose. *Radiology* 191: 379–382, 1994.
7. Strauss LG, Conti PS. The application of PET in clinical oncology. *J Nucl Med* 32: 623–648, 1991.
8. Boecker H, Ceballos BA, Bartenstein P, Weidl A, Siebner HR, Fassbender T, et al. Sensory processing in Parkinson's disease: investigation with 3D $H_2{}^{15}O$-PET. *Brain* 122: 1651–1665, 1999.
9. Badawi RD. 3D-mode acquisition in clinical PET. *Nucl Med Commun* 18: 801–804, 1997.
10. Yamamoto S, Amano M, Miura S, Iida H, Kanno I. Deadtime correction method using random coincidence for PET. *J Nucl Med* 27: 1925–1928, 1986.
11. Iida H, Miura S, Kanno I, Murakami M, Takahashi K, Uemura K. Design and evaluation of HEADTOME IV: a whole body positron emission tomography. *IEEE Trans Nucl Sci* NS-36: 1006–1010, 1989.
12. Fujiwara T, Watanuki S, Yamamoto S, Miyake M, Seo S, Itoh M, et al. Performance evaluation of a large axial field-of-view PET scanner: SET-2400W. *Ann Nucl Med* 11 (4): 307–313, 1997.
13. Zhang H, Alyafei S, Inoue T, Matsubara K, Tomiyoshi K, Endo K, et al. Comparison on two-dimensional and three-dimensional imaging characteristics of a whole-body PET scanner. *Eur J Nucl Med* 25: 1141, 1998.
14. Tanaka G. Japanese Reference Man 1988. *Annuals of Japan Radiological Society* 48: 509–513, 1988.
15. Lowe VJ, Duhaylonsod FG, Patz EF, Delong DM, Hoffman JM, Wolfe WG, et al. Pulmonary abnormalities and PET data analysis. A retrospective study. *Radiology* 202: 435–439, 1997.
16. Ollinger JM. Model-based scatter correction for fully 3D PET. *Phys Med Biol* 41: 153–176, 1996.